Appl. Phys. B 55, 164–170 (1992)

Applied Physics B Photophysics and Laser Chemistry

Laser-Induced Fluorescence Imaging in a 100 kW Natural Gas Flame

M. Versluis[1], M. Boogaarts[1], R. Klein-Douwel[1], B. Thus[2], W. de Jongh[2], A. Braam[2], J. J. ter Meulen[1], W. L. Meerts[1], and G. Meijer[1]

[1] Department of Molecular and Laser Physics, University of Nijmegen, Toernooiveld, NL-6525 ED Nijmegen, The Netherlands

[2] Department of Applied Physics, KEMA, Utrechtseweg 310, NL-6812 AR Arnhem, The Netherlands

Received 17 January 1992/Accepted 13 April 1992

Abstract. A tunable excimer laser at 248 nm (KrF) and 193 nm (ArF) has been used to monitor two-dimensional OH and NO distributions in the turbulent flame of a 100 kW natural gas burner. Spatially resolved fluorescence (spatial resolution better than 1.0 mm) from a 20 cm×20 cm area is collected under single shot conditions. We describe the problems encountered when laser-induced fluorescence imaging techniques are applied to large scale flames. Special experimental arrangements, imposed by the turbulent behavior of the flame we used, are also described.

PACS: 07.65, 82.40.Py, 42.80

During the last three decades the reduction of pollutants in combustion processes has received great interest [1]. Different diagnostic methods, e.g. emission spectroscopy [2] and the line-reversal method [3], have been applied in order to characterize temperatures of flames and densities of combustion species. About 15 years ago *laser* diagnostics entered the field of combustion with techniques as laser-induced fluorescence (LIF) [4] and coherent anti-stokes raman scattering (CARS) [4]. Recently other non-linear techniques such as degenerate four-wave mixing [5, 6] have been added to this list. Rayleigh scattering [7] and spontaneous Raman scattering in combination with LIF [8] are promising spectroscopic tools for flame diagnostics. So far, most techniques have been well experimented on at laboratory scale flames. Less experience has been obtained with the application of these techniques to larger scale flames, as for instance to flames in utility boilers of power plants.

In the Netherlands all power plants together are responsible for 15% of the total NO_x release in the Dutch atmosphere [9]. The combustion process in a utility boiler of a power plant, and its almost inevitable exhaust of nitric and sulfuric oxides, is mainly determined by the characteristics of the flames, such as temperature, species concentration distributions and local stoichiometry. The visualization of nitric oxide formation in the combustion process is of utmost importance for determining the optimum condition of the burner parameters, such as swirl and stoichiometry in order to develop a better, that is to say a cleaner, low NO_x-burner [10].

Laser-induced (predissociative) fluorescence (LI(P)F) is one of the most sensitive diagnostic techniques used in combustion, as has been demonstrated by various groups [11–16]. The detection of laser-induced predissociative fluorescence of OH [17] has an important advantage over detection of "normal" LIF of OH, because of its lack of collisional quenching at atmospheric pressures. When saturation of the electronic transition is avoided [18], LIPF gives the possibility of measuring densities and temperatures quantitatively, even in large two-dimensional areas. When OH is excited to the $A^2\Sigma^+(v' = 3)$ state with a tunable KrF excimer laser at 248 nm, the off-resonant fluorescence to unoccupied states is monitored, so there are no problems of fluorescence reabsorption [17]. The excimer lasers can work at a repetition rate of 50 Hz and the imaging of fluorescence with highly sensitive UV cameras with gated image intensifiers yield the opportunity to perform on-line measurements, e.g., changes of the burner configuration or of the burner conditions on the NO distribution are directly observed on the video monitor.

In this article we present two-dimensional laser-induced fluorescence measurements in a 100 kW natural gas flame. We have succesfully monitored the OH and NO distributions in a large area with a tunable excimer laser operating on KrF and ArF, respectively, in a single laser pulse. This article describes, from an application-oriented point of view, the problems encountered when laser-induced fluorescence imaging techniques are applied to large scale flames. The complicated experimental conditions, among others caused by the turbulent behavior of the flame we used, forced us to improvise and to improve our experimental apparatus. These special arrangements are also described.

1 Experimental Setup

The experimental setup is schematically given in Fig. 1. The different parts will be discussed below.

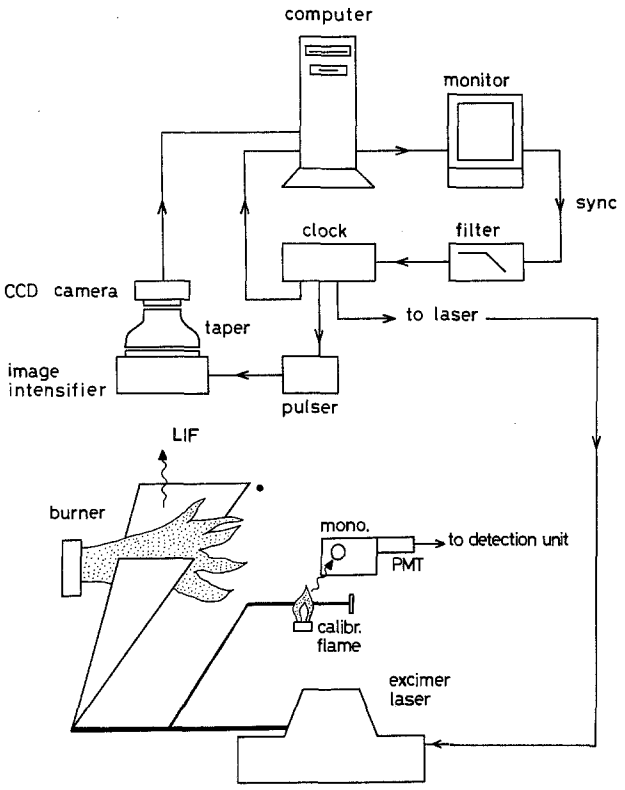

Fig. 1. The experimental setup. See text for further details

1.1 100 kW Burner

A photograph of the burner is shown in Fig. 2. The burner is a 1 : 100 down-scaled model of a 10 MW burner used in natural gas fired utility boilers. The burner burns horizontally and is located in a furnace supplied with a chimney. The walls of the furnace are insulated with aluminum oxide. The internal dimensions of the furnace are $0.7 \times 0.7 \times 2.0$ m. All experiments are done with a stretched natural gas flame. The flame has a typical diameter of 25 cm and its length is approximately 1.5 m. The natural gas is composed of about 80% methane and 14% nitrogen; the remaining 6% consist of higher hydrocarbons and also contain aromatic hydrocarbons such as toluene and benzene [19]. The natural gas is injected in the primary combustion air flow via six small pipes which have an effective opening of 4 mm^2 each. A secondary air flow is added to create a staged combustion [20]. The swirl of both air flows is adjustable in order to change the flame's shape and to create an internal recirculation zone in the furnace. We have measured at different stoichiometries[1] ranging from 0.9 to 1.5. The diameter of the flame is varied from 15 to 50 cm. Depending on the stoichiometry, soot is formed in the flame. We tried to avoid soot formation in the detection region and adjusted the swirl and air supply accordingly. The furnace has optical access via quartz windows. There are two Suprasil I windows, a 100 mm diameter laser entrance window and a 200 mm×200 mm laser exit window. A 200 mm×200 mm air-cooled Dynasil window on top of the furnace is used to transmit laser-induced fluorescence. All windows are 3 mm thick. The windows have to be cleaned with alcohol after several hours of operation because of deposition of aluminum oxides from the inside. All windows heat up within 15 minutes of burner operation and start to radiate strongly. The detection window is cooled with air to prevent heating of the electronic camera system.

[1] The stoichiometry is defined as the ratio of the actual oxygen concentration in the unburnt mixture to the oxygen concentration at the stoichiometric point, i.e. for complete combustion of the fuel to CO_2 and H_2O [21]

1.2 Laser System

A tunable excimer laser (Lambda Physik EMG 150 MSCT) is used to resonantly excite hydroxyl and nitric oxide radicals. The laser is operated on KrF (248 nm) for the OH measurements and on ArF (193 nm) for the NO measurements. The laser is grating-tunable over about 200 cm^{-1} within the gain profiles of the lasing transition of both excimers. The bandwidth of the laser is 0.4 cm^{-1} for KrF and 0.7 cm^{-1} for ArF. The laser is sometimes used in a modified setup without unstable resonator (or Cassegrain) optics to remove the fluorescence from species excited by the broadband background radiation of the laser [22]. However, often we need the full power of the laser and use Cassegrain optics in the amplifier. The output energy of the laser with unstable resonator optics is 250 mJ for KrF and 100 mJ for ArF. Tuning of the laser is performed by a stepper motor attached to a micrometer screw on the grating. To image a large part of the flame the rectangular laser output beam (25 mm×5 mm, divergence < 0.2 mrad) is transformed into a laser sheet of approximately 20 cm wide using a combination of spherical and cylindrical lenses. The thickness of the sheet depends on the imaging technique and the molecule under investigation (500 µm for OH and 5 mm for NO).

1.3 Calibration Flame

For calibration of the excitation wavelength, 10% of the laser beam is deflected by means of a MgF_2 beam splitter and directed into a small flame, where the excitation spectra of the species under investigation are recorded simultaneously. A monochromator-based system disperses the fluorescence and serves as a narrow-band filter. The monochromator (Jobin Yvon M25, 610 g/mm, resolution 1 nm) makes an unambiguous molecular assignment of the combustion species possible via detection of vibrationally resolved fluorescence [17]. A Bunsen burner (methane and air) is used as a calibration flame for the OH experiments, while an oxyacetylene welding torch is applied for the NO measurements. The laser passes through the flame approximately 2 cm above the flame front in both cases. The fluorescence of the specific molecules is collected with a $f = 100$ mm Suprasil I lens. The monochromator was set to transmit the OH: $A^2\Sigma^+(v' = 3) \rightarrow X^2\Pi(v'' = 2)$ off-resonant fluorescence at 295 nm in the OH experiment [17] and the NO: $D^2\Sigma^+(v' = 0) \rightarrow X^2\Pi(v'' = 3)$ off-resonant fluorescence at 208 nm in the NO experiment [23]. The transmitted photons are detected by a photomultiplier (EMI 9863 QB) and the signal is time averaged with a boxcar integrator with a gate width of approximately 50 ns. The averaged output of the integrator is recorded on a strip chart recorder.

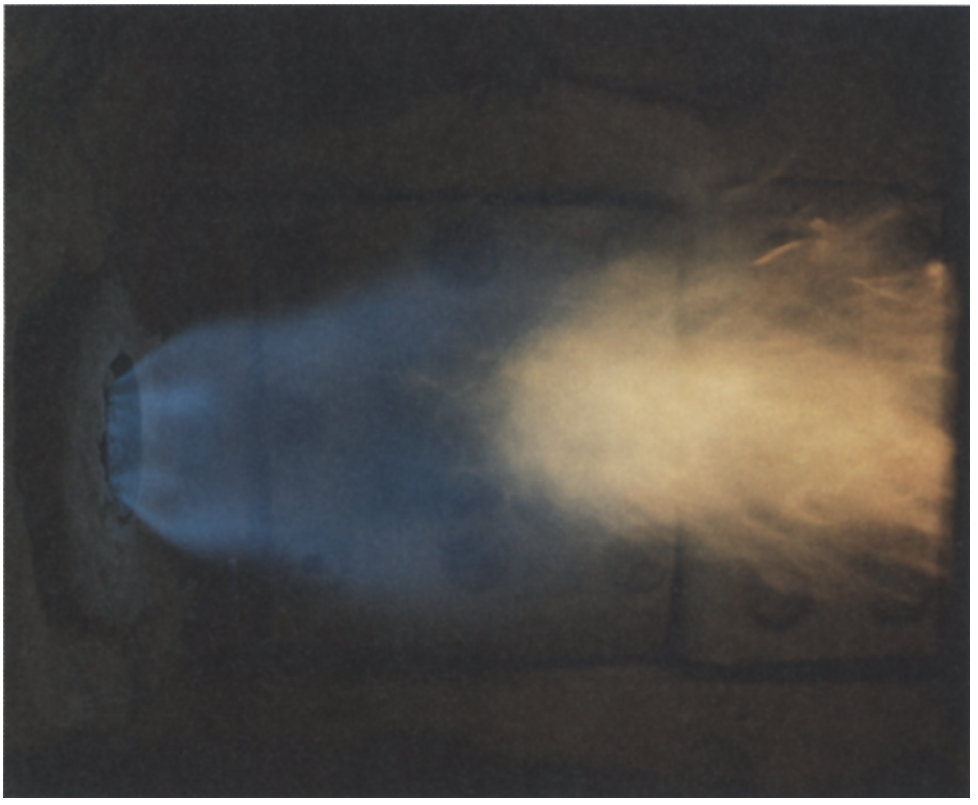

Fig. 2. Photograph of the natural gas flame. The natural gas is burnt with air. The flame has a diameter of approximately 30 cm and a length of 1.5 m. The burner is located in a furnace with optical access via quartz windows. The laser exit window is visible behind the flame

1.4 Detection System

The fluorescence emitted in the direction of the top of the furnace is collected with either an $f = 105$ mm UV-transparent objective (Nikon, UV-Nikkor, $f/4.5$) or a 4″ diameter $f = 100$ mm UV-grade fused silica lens. The fluorescence is focused on the photocathode of a gated image intensifier. Gating is performed with a modular gating unit suited for gating times down to 5 ns. Our gating time is typically 50 ns. The distance from the flame to the image intensifier is adjustable between 1.10 and 1.60 m. A CCD camera (Theta Electronic Systems) working in the European video rate mode (50 Hz) is attached to the phosphor screen of the image intensifier via a fiber optic taper. The video signal is digitized in a frame grabber (Matrox PIP-1024) installed in an IBM-compatible personal computer, equipped with an Intel 80386 microprocessor. Data processing and data acquisition is accomplished by home-written software. The video signal is simultaneously recorded on a VHS video recorder. Images are displayed on-line in a false color representation on a RGB color monitor. Processed images can be plotted on a color printer (HP-Paintjet).

1.5 Triggering

The CCD-camera is a free running unit which can not be triggered externally. Therefore, we choose the camera to trigger the experiment. The imaging board can be externally triggered by the synchronization pulse delivered by the camera. The output sync pulse of the board, attached also to the RGB monitor, is a 15 kHz pulse with a restart pulse every 20 ms. The latter pulse forces the monitor to start at the left-hand upper corner of the screen for a new image. This 50 Hz pulse is filtered from the 15 kHz sync pulse of the image processing board by means of a 500 Hz low-pass filter. The output of the filter is used to trigger a pulse/delay generator (SRS DG535). The pulse generator down converts the repetition rate to 10 Hz, a rate for optimum performance of the excimer laser. The output signals of the pulse generator are set to trigger the laser, the gating unit of the image intensifier and a serial port (RS-232) in the computer, which activates the software to process images for averaging and recording of spectra. This configuration allows to take synchronized snapshots from the camera[2].

2 Results

2.1 Small Scale Burner Experiments

The results of the measurements in the 100 kW flame are better understood if compared to the results from smaller flames. Therefore, we started our studies with 248 nm and 193 nm radiation in a Bunsen burner burning natural gas with air. The laser-induced fluorescence is monitored with the Nikon objective in front of the above described camera system. Bandpass filters are placed in front of the objective. A laser sheet of 200 μm thickness and 25 mm height is used for these measurements.

2.1.1 OH. Hydroxyl radicals (OH) are excited in a flame by inducing the $A^2\Sigma^+(v' = 3) \leftarrow X^2\Pi(v'' = 0)$ transition at 248 nm with a tunable KrF excimer laser [17]. The off-resonant fluorescence from the excited state to, predominantly, the $v'' = 2$ in the ground state near 295 nm is moni-

[2] Due to the synchronization the frame transfer best images have now also disappeared

tored. Rayleigh and Mie scattered laser light is filtered with a 2 mm thick Schott UG-11 glass filter. If a sheet of a tunable KrF laser passes through a Bunsen burner several laser-induced processes occur as indicated in Fig. 3. First, if the KrF laser is tuned to an OH resonance, fluorescence is induced on the outer sides of the flame. In addition, we observe the fluorescence of, so far, unidentified radicals produced shortly beyond the flame front. This fluorescence is not resonant with respect to the excitation laser wavelength and it is always present in the images. Furthermore, photodissociation of (aromatic) hydrocarbons, present in the natural gas, is detected via the fluorescence of the dissociation products. This fluorescence is located below the flame front where the gas has not burnt yet. Between the radicals produced on the flame front and the OH radicals in the flame, a region without fluorescence is present. This fluorescence pattern, from the burner head, where we have unburnt fuel, to the location where the combustion is completed, is seen back in every natural gas combustion process. Due to a hole in the beam profile of the KrF laser, less fluorescence is observed in the middle of the image.

With our software a rectangular area can be selected in the viewing region of the camera. The computer adds up all grey values within this specific region, and the sum, if wanted averaged over several pictures, is plotted on the computer monitor or on a plotter. The laser can be tuned within its gain profile and an excitation spectrum of a molecule that is spatially separated from other molecules in the flame can be recorded this way. This is demonstrated in Fig. 4 where the intensity in the white rectangle indicated in Fig. 3 is measured as the laser is scanned. All lines can be assigned to the well-known OH transitions [17]. Laser-induced fluorescence of $O_2(v'' = 6)$ [17] is also seen in the figure, since vibrationally hot oxygen is located at the same position in the flame. This option turned out to be important to recognize which species fluoresce in more complex flame types. Two dimensional pictures of OH excited from different rotational energy levels in the ground state can be processed to give a two-dimensional temperature profile of the flame. For a quantitative interpretation of absolute temperature measurements one should be aware of inherent difficulties, such as the variation of the predissociation lifetime with rotational quantum number [25]. In addition, the depletion of the ground state level population might complicate a quantitative analysis. The refilling through collisions of the probed level from neighbouring levels during the laser pulse causes an undesired enhancement of the fluorescence signal. Saturation of the electronic transition should therefore be avoided. Calibration measurements, using recently measured absolute predissociation lifetimes of the excited rotational states of OH [18, 26], are in progress to determine the absolute temperature distributions.

2.1.2 NO. The NO molecules are detected in a flame by exciting the $D^2\Sigma^+(v' = 0) \leftarrow X^2\Pi(v'' = 1)$ transition at 193 nm with a tunable ArF excimer laser [22, 23]. Off-resonant fluorescence from the excited state to the $v'' = 2, 3, 4$ in the ground state near 210 nm is monitored. Rayleigh and Mie scattered laser light is filtered with a highly reflective 193 nm/0° ArF laser mirror, transmitting $\lambda > 210$ nm. The non-resonant excitation of radicals on the flame front is more intense than the NO fluorescence. This can be seen in Fig. 5. The burner conditions are altered with respect to the OH measurements. The NO is distributed homogeneously on both sides of the flame front. The $D \leftarrow X$ transition of NO is saturated if the full power of the ArF laser is used

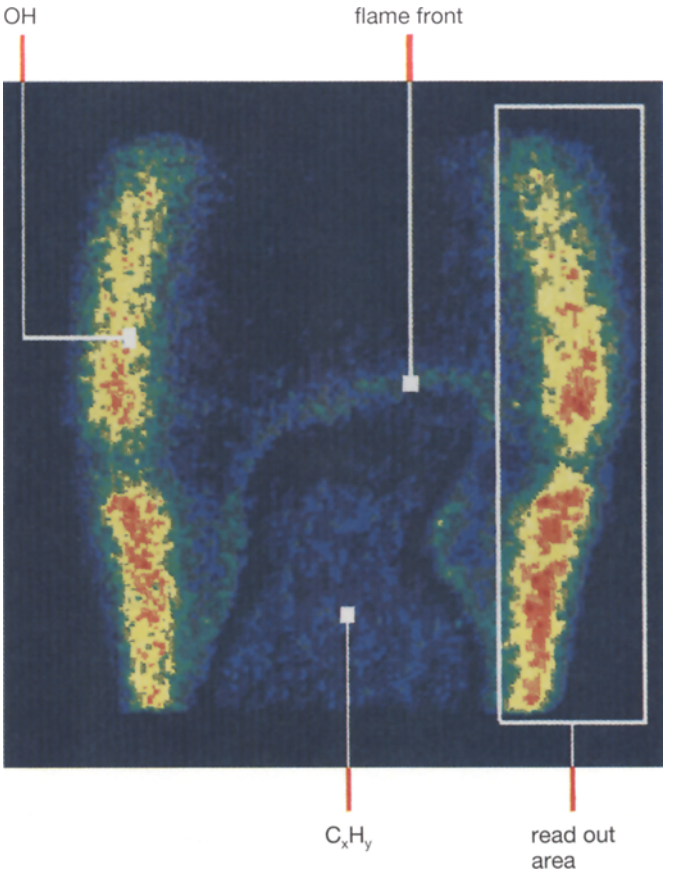

Fig. 3. A two dimensional KrF laser-induced fluorescence image from a Bunsen burner. The laser is tuned to the $P_2(8)$ resonance line of the OH: $A^2\Sigma(v' = 3) \leftarrow X^2\Pi(v'' = 0)$ transition. Due to a hole in the beam profile of the KrF laser, less fluorescence is observed in the middle of the image. Further details are discussed in the text

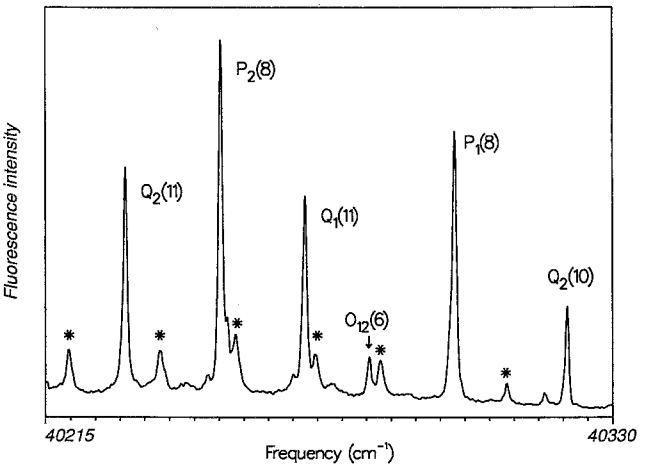

Fig. 4. The OH: $A^2\Sigma^+(v' = 3) \leftarrow X^2\Pi(v'' = 0)$ excitation spectrum measured with the camera as described in the text. Laser-induced fluorescence of $O_2(v'' = 6)$, denoted with asterisks, is also seen in the figure since vibrationally hot oxygen is located at the same position in the flame

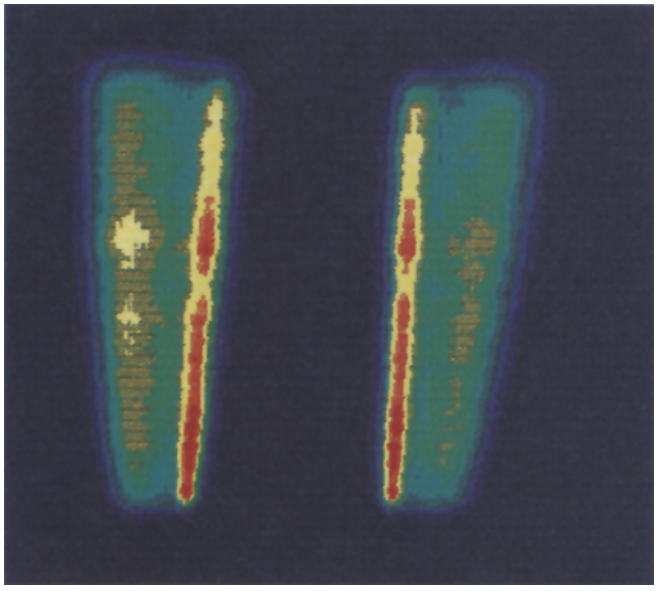

Fig. 5. A two dimensional ArF laser-induced fluorescence image from a Bunsen burner. The laser is tuned to the $R_1(26.5)$ and $Q_1(32.5)$ resonance line of the NO: $D^2\Sigma^+(v'=0) \leftarrow X^2\Pi(v''=1)$ transition. Nitric oxide is distributed homogeneously on both sides of the flame front

to excite the molecules. The sheet can therefore be widened to excite more molecules, and hence, to increase the signal level.

2.2 100 kW Burner Experiments

2.2.1 OH. In the upper part of Fig. 6 a single laser shot image is shown when the laser is tuned to the $P_2(8)$ resonance line of the OH: $A^2\Sigma^+(v'=3) \leftarrow X^2\Pi(v''=0)$ transition. A laser sheet of 500 µm thickness and 20 cm width is used. The energy of the KrF laser is 100 mJ per pulse, leading to an excitation condition near saturation. The OH radicals are distributed in a narrow line along the flame front. The fluorescence is collected from a region as big as 16 × 14 cm at about 8 cm from the burner head. Most prominent, however, is the broadband non-resonant fluorescence of the photodissociated hydrocarbons under the flame front as seen before in the Bunsen burner. It will be possible to suppress this emission light to a great extent by applying special fluorescence filtering. The lower part of Fig. 6 shows a single laser shot spatial distribution while the laser is tuned off the OH resonance. The photodissociated hydrocarbon fluorescence remains, while the slim line along the flame front disappears. It is important to use a high-quality objective in front of the camera to detect the spatially confined OH fluorescence. Using normal lenses the image is blurred and dominated by the emission of the hydrocarbons. The flame is extremely turbulent. The OH contour can, however, be followed all around the flame at every laser shot. The signal-to-noise ratio for OH detection in a single-shot image is approximately 40. Temperature fields can not be measured under such turbulent conditions, unless one has access to two laser systems and two camera systems. Even then only moderate information is gained on the temperature distribution in such flames, since only a small area is covered by the OH molecules.

2.2.2 NO. The OH signals were strong and easily measured compared with our work in this burner concerning nitric oxide field distributions. We encountered problems due to absorption of the 193 nm laser radiation. The total integrated absorption of the flame and its surroundings amounts up to 70%. In air oxygen strongly absorbs due to the O_2: $B^3\Sigma_u^-(v'=4) \leftarrow X^3\Sigma_g^-(v''=0)$ transition [27], which gives rise to reduced laser action at five frequencies in the tuning range of the ArF laser. The O_2 absorption lines are broadened due to predissociation of the vibrational levels in the $B^3\Sigma_u^-$ state. The problem of absorption can be solved by flushing the laser beam path with nitrogen. A more serious problem is the absorption of laser radiation in and around the flame and successive disturbing fluorescence due to O_2 resonances starting from the vibrational levels $v''=2$ and 3 in the $X^3\Sigma_g^-$ ground state [24, 27]. The hot surroundings of the flame contain vibrationally excited ground state oxygen molecules, especially when the flame is situated in a closed environment. From the 50 transitions in NO in the tuning range of the ArF laser the $R_1(26.5)$ and $Q_1(32.5)$, which lie both at a frequency of 51712.5 cm^{-1} [22], can be excited having the smallest effect of the O_2 resonances. The transition frequencies and absorption intensities of the vibrationally hot oxygen resonances in the tuning range of the ArF excimer laser have been carefully examined by Lee et al. [28].

The two aforementioned resonances of NO are the resonances we use to measure the NO distribution in the 100 kW flame. The use of a 4″ diameter fused silica lens turned out to be essential to collect enough photons onto the photocathode of our camera system. As a result of this we could increase the thickness of our laser sheet to approximately 5 mm without loosing our spatial information. With high power densities the fluorescence is saturated; more molecules (in a bigger volume due to a thicker sheet) simply increase the signal level. The energy of the ArF laser is 10 mJ per pulse. The excitation condition for the fluorescence is therefore linear. Excitation spectra measured with our special software option described in Sect. 2.1.1 turned out to be essential too to find the location of highest NO concentration in the flame. Several areas within the viewing region of the camera were scanned for NO presence. The use of the calibration flame, to check whether the laser is on a NO resonance, was very important because of the enormous additional fluorescence from $O_2(v''=2,3)$ in and around the 100 kW flame.

A typical NO field distribution is shown in Fig.7. The image is averaged over 100 laser shots. The fluorescence is collected from a region as big as 16 × 14 cm at about 7 cm from the burner head. The absorption of laser radiation is clearly seen in the figure. The image is not corrected for this absorption, since it is almost impossible to determine the exact laser fluence at a given point in the flame. Single shot NO distributions are obtained, too. Again the distribution is extremely turbulent. The signal-to-noise ratio for NO detection in a single shot image is 15. The Kolmogorov microscale of turbulence for this flame is calculated to be 400 µm [29]. Therefore, with a sheet thickness of 5 mm, the single shot images have lost their structural information

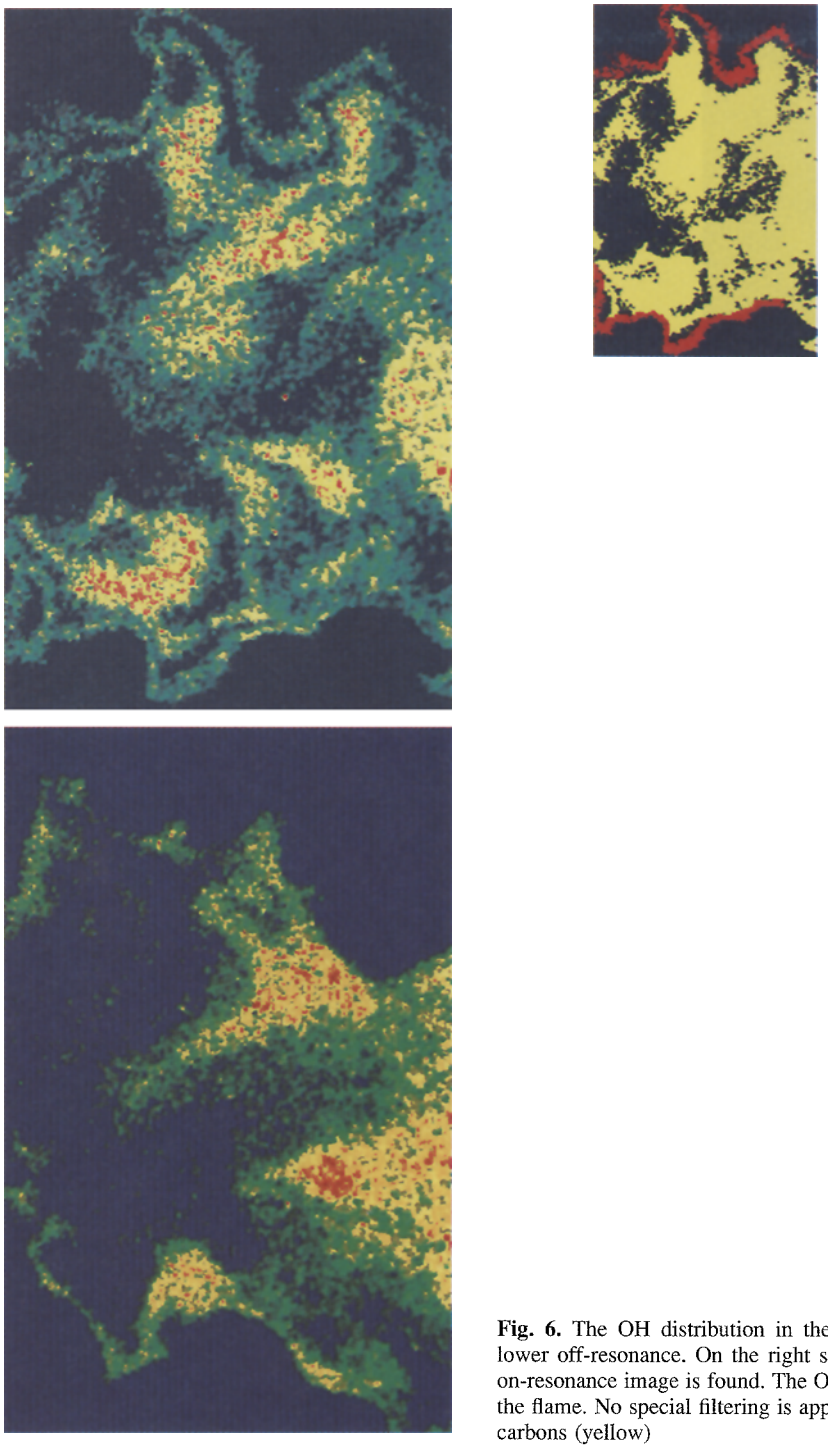

Fig. 6. The OH distribution in the 100 kW flame. Upper image on the $P_2(8)$ resonance, lower off-resonance. On the right side of the upper image a schematic reproduction of the on-resonance image is found. The OH radicals (red) are distributed along a small line around the flame. No special filtering is applied to remove the broadband fluorescence of the hydrocarbons (yellow)

concerning the smallest turbulent eddies in the flame. The results give only a qualitative view of the turbulences associated with this flame. From the number of photo-electrons a rough estimate indicates a NO concentration in the 100 ppm range [30], in accordance with what is expected for these type of furnaces. We have changed the stoichiometry of the flame, which is known to lead to a variation of NO production, while simultaneously monitoring the on-line NO fluorescence in the flame and the NO_x emission in the chimney with a probe. We find a qualitative correlation between the probe data and the NO fluorescence data. Less NO in the flame corresponds to a smaller amount of NO_x emission in the chimney. As a first result of our experiments the design of the burner has been improved. The flame appears more stable and produces a remarkable smaller amount of NO_x, as was checked with the probe. To verify this, however, one would need quantitative NO concentration fields, requiring also instantaneous temperature fields, for the different burner designs and correlated exhaust data, which lie beyond our present experimental possibilities.

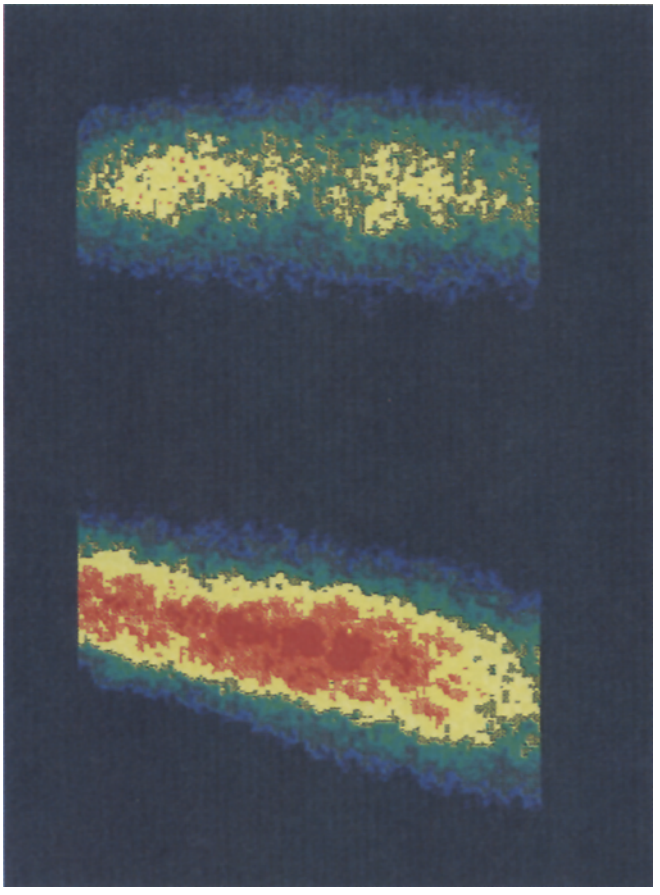

Fig. 7. The NO distribution in the 100 kW flame. The laser is tuned to the $R_1(26.5)$ and $Q_1(32.5)$ resonance line of the $D \leftarrow X$ transition. The image is averaged over 100 laser shots. The absorption of the laser radiation (from the bottom to the top) is clearly seen in the figure

3 Summary

We have applied the technique of laser-induced fluorescence in a relatively large natural gas flame. Density field distributions of OH and NO have been measured. An attempt to measure temperature fields was unsuccessful, due to the turbulent behavior of the flame and due to the small area in which the OH molecules are produced. More general, the OH and NO images show directly that care has to be taken with the interpretation of any type of temperature measurements, due to the extreme turbulent character of the flame.

Acknowledgements. The technical assistance of John Holtkamp is gratefully acknowledged. We thank John van Bladel for valuable assistance during the development of our special software. We thank La Vision GmbH, Göttingen (FRG) for important contributions concerning the electronic camera system. Peter Andresen and co-workers are acknowledged for helpful suggestions and valuable discussions. Gerard Meijer acknowledges the support of the Koninklijke Nederlandse Academie der Wetenschappen (KNAW). This work has been made possible by the financial support of the Samenwerkende Electriciteits-Productiebedrijven (NV SEP) and the Stichting voor Technische Wetenschappen (STW).

References

1. I. Glassman: Combustion (Academic Press, London 1987) 318–385
   M.L. Elder, J.D. Wineforder: Proc. Analyt. Atom Spectrosc. **6**, 292–427 (1983)
2. A.G. Gaydon: *The spectroscopy of flames,* 2nd edn. (Chapman & Hall, London 1974) pp. 182–220
3. A.G. Gaydon, H.G. Wolfhart: Flames, their structure, radiation and temperature (Chapman & Hall, London 1970) pp. 239–242
   C.Th.J. Alkemade, Tj. Hollander, W. Snelleman, P.J.Th. Zeegers: Metal vapours in flames (Pergamon, Oxford 1982) pp. 315–329
4. A.C. Eckbreth: Laser diagnostics for combustion temperature and species (Abacus, Cambridge, MA 1988)
5. T. Dreier, D.J. Rakestraw: Opt. Lett. **15**, 71–74 (1990)
6. P. Ewart, M. Kaczmarek: Appl. Opt. **30**, 3996–3999 (1991)
7. M.B. Long, B.F. Weber, R.K. Chang: Appl. Phys. Lett. **34**, 22-24 (1979)
   R. Miles, W. Lempert: Appl. Phys. B **51**, 1–7 (1990)
8. J.A. Wehrmeyer, T.S. Cheng, R.W. Pitz: Appl. Opt. (in press 1991)
9. The Dutch National Environmental Policy Plan, Part II, National Institute for Public Health and Environmental Protection (RIVM) (1990)
10. A. Braam, H. Hulshof, W. de Jongh, B. Thus: Proc. of the First Conference on Combustion and Environment (Vilamoura, Portugal 1991) pp. 19–24
11. R.K. Hanson, J.M. Seitzman, P.H. Paul: Appl. Phys. B **50**, 441–454 (1990)
12. P. Andresen, G. Meijer, H. Schlüter, H. Voges, A. Koch, W. Hentschel, W. Oppermann, E. Rothe: Appl. Opt. **29**, 2392–2404 (1990)
13. R. Suntz, H. Becker, P. Monkhouse, J. Wolfrum: Appl. Phys. B **47**, 287–293 (1988)
14. An overview of recent LIF applications is found in: Appl. Phys. B **50**(6) (1990); B **51**(1) (1990)
15. A. Koch, A. Chryssostomou, P. Andresen, W. Bornscheuer: Submitted (1991)
16. A. Chryssostomou, H. Voges, W. Reckers, P. Andresen, P. Krogmann, K.-A. Bütefisch, H. Wolfrum: Report No. 1/340/1990, Laser Laboratorium Göttingen (Göttingen 1990)
17. P. Andresen, A. Bath, W. Gröger, H. Lülf, G. Meijer, J.J. ter Meulen: Appl. Opt. **27**, 365–378 (1988)
18. J.A. Gray, R.L. Farrow: J. Chem. Phys. **95**, 7054–7060 (1991)
19. Private communication with Gasunie, the Netherlands
20. D. Mormile: Proc. EPA and EPRI Symposium on Stationary Combustion NO_x-control (New Orleans 1987) Chap. 42, pp. 1–18
21. A.G. Gaydon: The spectroscopy of flames, 2nd edn. (Chapman & Hall, London 1974) p. 159
22. M. Versluis, M. Ebben, M. Drabbels, J.J. ter Meulen: Appl. Opt. **30**, 5229–5234 (1991)
23. A.M. Wodtke, L. Hüwel, H. Schlüter, G. Meijer, P. Andresen, H. Voges: Opt. Lett. **13**, 910–912 (1988)
24. A.M. Wodtke, L. Hüwel, H. Schlüter, H. Voges, G. Meijer, P. Andresen: J. Chem. Phys., **89**, 1929–1935 (1988)
25. M.L. Sink, A.D. Bandrauk, R. Lefebvre: J. Chem. Phys. **37**, 4451–4459 (1980)
26. D.E. Heard, D.R. Crosley, J.B. Jeffries, G.P. Smith, A. Hirano: J. Chem. Phys. (submitted 1991)
27. K. Yoshino, D.E. Freeman, W.H. Parkinson: J. Phys. Chem. Ref. Data **13**, 207–227 (1984)
28. M.P. Lee, R.K. Hanson: J. Quant. Spectrosc. Radiat. Transfer **36**, 425–440 (1986)
29. H. Tennekes, J.L. Lumley: *First course in turbulence*, 3rd edn. (Mass. Institute of Technology, Boston 1974)
30. M. Boogaarts: Internal Report, Dept. of Molecular and Laser Physics, University of Nijmegen (1991)